

Josephson diodes induced by the loop current states

Qi-Kai Shen¹ and Yi Zhang^{1,2,*}

¹Department of Physics and Institute for Quantum Science and Technology, Shanghai University, Shanghai 200444, China

²Shanghai Key Laboratory of High Temperature Superconductors and International Center of Quantum and Molecular Structures, Shanghai University, Shanghai 200444, China

(Dated: December 31, 2024)

We study the diode effect of the supercurrent in the Josephson junctions with the loop current states as the tunneling barrier. The loop current states are realized by the Haldane model which preserves the inversion symmetry and thus forbids the diode effect. We demonstrate how the inversion symmetry can be broken in the monolayer and bilayer systems. In the monolayer system, inversion symmetry can be broken by either introducing a sublattice staggered potential for the Haldane model or introducing a modified Haldane model, and in the bilayer system, it can be broken by either stacking the two layers with opposite current directions or by directly applying an electric field perpendicular to the layers. We further show that the diode efficiency can be tuned by the interlayer coupling and the strength of the electric field or interlayer voltage. Our results provide another route to realize the Josephson diode effect by breaking the time-reversal symmetry through the loop-current states.

Introduction.— Superconducting diode effect (SDE) refers to the phenomenon where critical supercurrents flowing in opposite directions have different magnitudes. This non-reciprocal transport effect in the superconducting system can play a similar role as the diodes formed by the p-n junctions in the semiconductor industry and has potential applications in the development of dissipationless electronics [1, 2].

SDE has been observed experimentally in numerous superconducting systems [3–13]. Such diode effect is also realized in the various Josephson junction (JJ) systems [14–24], which is named the Josephson diode effect (JDE). It provides an extra knob to realize and tune the diode effect by designing the proper barrier layer of the JJs.

On the side of theoretical development, JDE was first proposed based on the electron and hole-doped superconductors (SC) in analog to the semiconducting p-n junctions [25]. From the symmetry point of view, both SDE and JDE require the system to break both inversion and time-reversal symmetry. These special JJs with both symmetry broken were intensively studied [26–38]. One class of such JJs is called Josephson ϕ_0 junction, which provides a possible mechanism to realize the JDE. More recently, as stimulated by the experimental observations, numerous theoretical proposals [39–70] have been suggested for these effects. Moreover, the diode effect for the spin transport in the JJs is also proposed [71, 72].

While most of the realizations of the SDE/JDE require a finite external magnetic field or internal net magnetic moment to break the time-reversal symmetry, recent observations of the field-free diode effect in the JJs [14] and SC bulk [7] significantly expand the potential scope for this phenomenon but at the same time call for new theoretical mechanisms to realize it. Besides the systems with the magnetic field, the loop current states are distinct phases of matter that break the time-reversal symmetry, which are extensively studied in different systems, ranging from the Haldane model [73] on the honeycomb lattice to the various forms of flux phases in the square lattice [74–80] and triangular lattice [81–84]. The recent discovery of the exotic charge density wave in nonmag-

netic AV_3Sb_5 ($A = K, Rb, Cs$) [85–93] provides another possible material realization of the loop current states [94–102]. In this work, we propose a theoretical model to realize the JDE using the loop current states as the tunneling barrier of the JJ, which serves as the source of the time-reversal symmetry breaking. We construct the loop current states in the honeycomb lattice with monolayer and bilayer systems. For the monolayer case, JDE can be realized either by introducing a potential difference for the two sublattices or by modifying the current directions of the Haldane model that breaks the inversion symmetry directly. For the AB-staked bilayer case, JDE can be induced by either stacking the two layers with opposite loop currents or applying an out-of-plane electric field. For the bilayer system, we further analyze the effect of the interlayer coupling and displacement field on the diode efficiency.

Tight-binding Models.— As the basic building block of the tunneling barrier of the JJ, we start with the Haldane model (HM) [73] on a honeycomb lattice containing two different types of atoms denoted A and B, as shown by the solid line in Fig. 1(a). The tight-binding Hamiltonian can be written as

$$H_m = -t \sum_{\langle i,j \rangle \sigma} c_{i\sigma}^\dagger c_{j\sigma} - t_1 \sum_{\langle\langle i,j \rangle\rangle \sigma} e^{-i v_{ij} \phi} c_{i\sigma}^\dagger c_{j\sigma} \quad (1)$$

where $i(j)$ labels the lattice sites and σ is the electron spin index. The operators $c_{i\sigma}(c_{i\sigma}^\dagger)$ represent the annihilation (creation) operators of fermions located at site i with spin σ . Moreover, t is the nearest-neighbor (NN) hopping and $t_1 = 0.4t$ denotes the amplitude of the next-nearest-neighbor (NNN) hopping. The complex NNN hopping breaks time-reversal symmetry by forming a loop current state, with $v_{i,j} = 2/\sqrt{3}(\hat{\mathbf{d}}_1 \times \hat{\mathbf{d}}_2)_z = \pm 1$, where $\hat{\mathbf{d}}_1$ and $\hat{\mathbf{d}}_2$ are the unit vectors along the two bonds that constitute the NNN bonds from site i to site j . The signs of the NNN hopping phase are schematically shown in Fig. 1(b), which is positive along the arrow direction. From the sign pattern, we can see that the bonds along the same direction, but consisting of different types of atoms, have hoppings with opposite phases, which

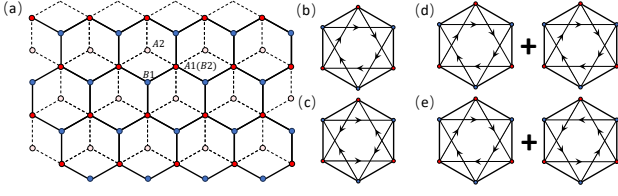


FIG. 1. (a) Schematic plot of the bilayer honeycomb lattice. The first layer is characterized by atoms labeled as A1 and B1, connected by solid lines, while the second layer is indicated by A2 and B2 atoms, connected by dashed lines. The stacking of A1 atoms from the first layer with B2 atoms from the second layer gives rise to the bilayer HMs. (b) In the HM, the NNN hopping directions of atoms A and B are opposite. (c) In the MHM, the NNN hopping directions of atoms A and B are the same. (d) Two HMs are stacked with the same loop current directions. (e) Two HMs are stacked with opposite loop current directions.

preserves the inversion symmetry. Since the inversion symmetry has to be broken to achieve the JDE, we further consider the modified Haldane model (MHM) [103], where the sign of the hopping phase of the bonds consisting of atom B are reversed, as illustrated in Fig.1(c). Therefore, in the MHM, both time-reversal and inversion symmetry are broken, which meets the basic symmetry requirement to realize the JDE.

Besides the monolayer system, we also consider the bilayer HMs, where the two layers of the honeycomb lattice are Bernal stacked, with one layer's A atoms stacked with the other layer's B atoms as shown in Fig.1(a). The Hamiltonian for the bilayer system can thus be written as

$$\begin{aligned}
 H_b &= H_1 + H_2 + H_{12} \\
 H_l &= -t \sum_{\langle i,j \rangle \sigma} c_{i l \sigma}^\dagger c_{j l \sigma} - t_\perp \sum_{\langle\langle i,j \rangle\rangle \sigma} e^{-i v_{ij} \phi} c_{i l \sigma}^\dagger c_{j l \sigma} \\
 H_{12} &= -t_\perp \sum_{i, \sigma} c_{i, A1 \sigma}^\dagger c_{i, B2 \sigma} + h.c.
 \end{aligned} \quad (2)$$

where l is the layer index, H_l represents the Hamiltonian for each layer, and H_{12} corresponds to the coupling between the two layers. Here, we assume that only the atoms stacked on top of each other between the two layers (A1-B2) contribute to this interlayer coupling t_\perp . The introduction of the extra layer brings more freedom to manipulate the symmetry of the system. Here, we consider the loop current pattern of each layer forms the original HM, which is demonstrated to be more stable in a mean-field calculation [104]. Then, the remaining degree of freedom is the relative orientation of the loop current of the two layers. When the two layers have the loop current with the same orientation as depicted in Fig. 1(d), the inversion symmetry remains preserved and the bilayer system has similar properties as the monolayer HM. In order to break the inversion symmetry in this state, an electric field perpendicular to the layers can be introduced. On the other hand, when the orientations of the loop current are opposite for each layer as shown in Fig. 1(e), the inversion symmetry is broken by having an odd parity with respect to two layers. This is the magnetoelectric state theoretically proposed in the bilayer

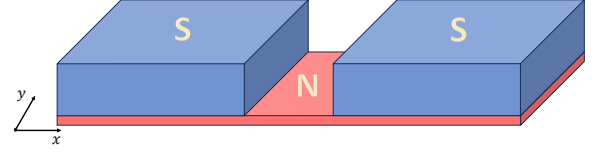


FIG. 2. Schematic of a planar Josephson junction in the $x - y$ plane. The blue region signifies the superconducting region (S), while the red region represents the normal region (N). The periodic boundary condition is used for the y -direction and the Josephson current flows in the x -direction.

honeycomb lattice with NNN repulsion [104].

Construction of the Josephson junction.— We next construct the planar Josephson junction using the monolayer and bilayer systems as the tunneling barrier. As depicted in Fig.2, this can be achieved by placing two s-wave superconductors (blue) on a two-dimensional material with loop current order (red). Due to the proximity effect, the two-dimensional material underneath the superconductors becomes superconducting. The region without superconductors in between remains in the normal state, thus forming a Josephson junction. Since the translation symmetry is preserved in the y -direction, we adopt the periodic boundary condition in this direction. In the y -direction, we consider unit cells $N_y = 100$, while in the x -direction, we have 20 layers for the left superconducting region, 2 layers for the middle normal region, and 20 layers for the right superconducting region.

The Hamiltonian of this Josephson junction, structured upon a honeycomb lattice, can be expressed as follows:

$$\begin{aligned}
 H &= H_{SL} + H_{SN} + H_N + H_{NS} + H_{SR} \\
 H_{SL} &= H_0 + \Delta e^{i\varphi} \sum_i c_{i\uparrow}^\dagger c_{i\downarrow}^\dagger + h.c. - \mu_0 \sum_{i, \sigma} c_{i\sigma}^\dagger c_{i\sigma} \\
 H_N &= H_0 - \mu_0 \sum_{i, \sigma} c_{i\sigma}^\dagger c_{i\sigma} \\
 H_{SR} &= H_0 + \Delta \sum_i c_{i\uparrow}^\dagger c_{i\downarrow}^\dagger + h.c. - \mu_0 \sum_{i, \sigma} c_{i\sigma}^\dagger c_{i\sigma}
 \end{aligned} \quad (3)$$

where H_0 represents the Hamiltonian of monolayer or bilayer system, as derived from either Eq.S2 or Eq.S3. H_{SL} and H_{SR} are the Hamiltonians of the superconducting regions. H_N represents the Hamiltonian of the non-superconducting region. H_{SN} and H_{NS} represent the spin-conserving hoppings between the superconducting and normal sections which include both the NN and NNN hoppings and take the same values and patterns as those in the normal region. The superconducting phase bias for the JJ is assigned to the left superconducting region as φ so that the phase in the right superconducting region is set to 0. The amplitude of the order parameter is taken as $\Delta = 0.2t$ for all calculations in this paper. μ_0 represents the chemical potential of the entire material, which is set to $-0.4t$ in the bilayer model, and set to 0 in the monolayer system.

The Josephson current flows in the x -direction and the supercurrent through the junction is related to the total energy of

the system by [105]

$$I(\varphi) = \frac{2e}{\hbar} \partial_\varphi \sum_n f(\epsilon_n(\varphi)) \epsilon_n(\varphi) \quad (4)$$

where ϵ_n represents the n th eigenvalue of the total Hamiltonian H and $f(x)$ denotes the Fermi-Dirac distribution function, with the temperature set to be $10^{-3}t$ through the whole paper. In Eq. 4, while considering the contribution of the superconducting current, all states are included.

The current-phase relationship.— We construct the JJs with both the monolayer and bilayer systems as the tunneling barrier. Depending on the orientation of the junction, we name the JJ as a zigzag (armchair) JJ, if the edge of the junction along the current flow direction has a zigzag (armchair) shape. For the monolayer case, when the tunneling barrier is constructed with the HM, the current-phase relation (CPR) shows no diode effect, where the critical current for the positive and negative directions have the same magnitude [106]. This is expected since the loop current pattern in the HM preserves the inversion symmetry, which precludes the emergence of the JDE. One way to break this inversion symmetry is to introduce a staggered lattice potential within the unit cell of HM, which can be described by an extra term $H_s = V_s \sum_{i,\sigma} (c_{i,A\sigma}^\dagger c_{i,A\sigma} - c_{i,B\sigma}^\dagger c_{i,B\sigma})$. This term is added to Eq. S2 which enters the Hamiltonian of the JJ as H_0 in Eq. S1. The staggered potential can be realized by placing the material on a substrate with a honeycomb structure, such as hexagonal BN, where the two sublattices consist of different atoms. The CPR for both types of the JJ is shown in Fig. 3(a, b). Indeed, we can see that the zigzag JJ shows the diode effect where the magnitude of the critical current for both directions differs from each other, i.e., $I_c^+ \neq |I_c^-|$ as shown in Fig. 3(a). Moreover, a finite Josephson current is achieved for the vanishing phase bias φ , which is directly related to the breaking of both inversion and time-reversal symmetry in this system. However, the CPR for the armchair JJ does not show any non-reciprocal effect. We can understand the different behaviors of the two types of JJs from the symmetry argument. From the symmetry point of view, if the system is invariant under a certain operation that also changes the sign of the current operator, the state of the system with a positive current is always connected to another state with its current reversed by this operation. This means the critical current must have the same magnitude for opposite directions, which causes the absence of the JDE. Since both time-reversal and inversion change the sign of the current operator, the JDE requires both symmetries to be broken. However, even in a system with both symmetries broken, as long as there exists a symmetry that changes the sign of the current operator, the JDE is still strictly forbidden. For the armchair JJ with staggered potential, this symmetry is $M_b C_2 \mathcal{T}$, where M_b is the mirror reflection about the plane perpendicular to the armchair edge [106], C_2 is the 2-fold rotation about the axis perpendicular to the JJ and \mathcal{T} is the time-reversal operator. Since all three operations change the current direction of the armchair JJ, this combined symmetry operation does change the sign of the current operator

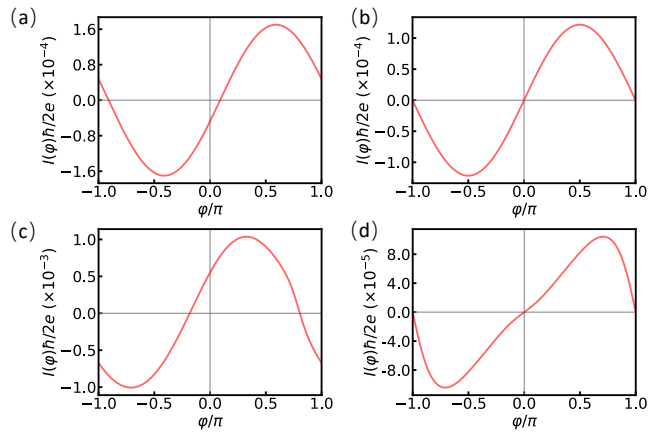


FIG. 3. The CPR in the monolayer honeycomb lattice. The JJ is constructed by the HM with staggered lattice potential V_s for (a) and (b), and constructed by the MHM for (c) and (d). (a) and (c) represent the zigzag JJ, which exhibits the diode effect. In contrast, (b) and (d) represent the armchair JJ, which does not show any diode effect. Parameters are taken as $t = 1$, $t_1 = 0.4t$, $\phi = \pi/4$, $V_s = 0.2t$, $\Delta = 0.2t$, $\mu_0 = 0$

in the armchair JJ and thus forbids the JDE.

On the other hand, if the tunneling barrier is constructed with the MHM, where the inversion symmetry is explicitly broken by the loop current pattern, we also expect the JDE to show up. As shown in Fig. 3(c, d), we again find that the JDE only shows up for the zigzag JJ. This time, it is the M_b symmetry that prevents the JDE from taking place in the armchair JJ.

We next consider the JJs constructed with the bilayer HMs. Based on the analysis of the monolayer case, we can see that breaking the inversion symmetry becomes the key factor in realizing the JDE in the system since the time-reversal symmetry is already broken. We first consider the case where the orientation of the loop current for the two layers is the same, which still preserves the inversion symmetry and thus prevents the emergence of the JDE. In this system, the inversion symmetry can be broken by applying an external electric field perpendicular to the layers, resulting in a potential difference between the two layers. In our calculation, this effect is described by a layer-dependent potential term $H_U = U/2 \sum_{l,i,\sigma} (-1)^l c_{il\sigma}^\dagger c_{il\sigma}$ which is added to the tunneling barrier part of the Hamiltonian in Eq. S1. In this case, the JDE again shows up only for the zigzag JJ. The CPR for the zigzag JJ with $U = 0.5$ is shown in Fig. 4(a), which clearly shows the JDE induced by the external electric field.

Besides the case where the inversion symmetry is broken by the external field, we next consider the bilayer magnetoelectric state where the orientations of the loop current of the two layers are opposite to each other so that the inversion symmetry is broken intrinsically. In this case, the JDE can be realized without the help of an external field as shown in Fig. 4(b) for the CPR of the zigzag JJ. The CPR for the armchair JJ again

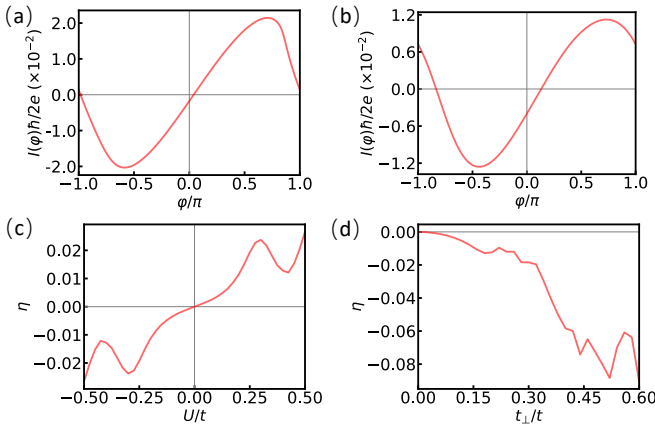


FIG. 4. The CPR in bilayer zigzag HMs. (a) The JJ is formed by stacking two HMs with the same loop current direction. Inversion symmetry is broken by applying voltage ($U = 0.5$) between the two layers. (b) The JJ is formed by stacking two HMs with opposite loop current directions. (c) The diode efficiency η as a function of the applied voltage U in bilayer HMs with the same loop current directions. (d) The diode efficiency η as a function of the inter-layer hopping t_{\perp} in bilayer HMs with opposite loop current directions. Parameters are taken as $t = 1$, $t_1 = 0.4t$, $t_{\perp} = 0.4t$, $\phi = \pi/4$, $\Delta = 0.2t$, $\mu_0 = -0.4t$

does not show any diode effect. A thorough symmetry analysis for the absence of the JDE in the armchair JJ is provided in the supplemental material [106].

Tuning the diode efficiency.— To investigate the factors influencing the diode effect, we use the diode efficiency factor η to quantify the extent of the diode effect. It is defined as:

$$\eta = \frac{I_c^+ - |I_c^-|}{I_c^+ + |I_c^-|} \quad (5)$$

where I_c^+ (I_c^-) is the critical current along the positive (negative) direction, and η reflects the strength of the diode effect. For the bilayer HMs, the inversion symmetry is broken by applying the interlayer voltage U for the case with the same loop current direction and the interlayer hopping t_{\perp} for the case with opposite directions of the loop current breaks the independent C_2 rotation symmetry, both of which result in the JDE. Therefore, it is natural to investigate the effects of U and t_{\perp} on the diode efficiency. For the zigzag JJ constructed with bilayer HMs with the same loop current direction, we vary the voltage U from -0.5 to 0.5 to investigate its impact on the diode effect. As shown in Fig.4(c), when the magnitude of U is small, the diode efficiency η monotonically increases with U and changes signs as U changes signs. In this region, the polarity and the strength of the diode efficiency can be well controlled by the external electric field. This is reasonable since the diode efficiency should increase with the strength of the inversion symmetry breaking as the time-reversal symmetry is fixed by the loop current order and the external voltage is the only source of the inversion symmetry breaking. As the magnitude of U further increases, the behavior of the diode efficiency becomes complicated as the band structure of the

system is significantly changed by the large value of U .

We next study the effect of the interlayer coupling t_{\perp} on the diode efficiency for the JJ constructed by the bilayer HMs with the opposite loop current directions. As shown in Fig.4(d), the diode effect disappears when t_{\perp} vanishes, which is due to the fact the two layers are decoupled in this limit and each layer has its own C_2 rotation symmetry that prevents the emergence of the JDE. Then, as t_{\perp} increases from 0 to 0.6, the magnitude of η monotonically increases with t_{\perp} when it is weak and starts to exhibit oscillations when it further increases. This is because t_{\perp} breaks the independent C_2 rotation symmetry of the two layers by locking the two layers together keeping the Bernal stacking structure, leading to the emergence of the JDE. Therefore, t_{\perp} plays a similar role here as the voltage U in the case with the same loop current direction for the two layers.

Discussion.— In summary, we have demonstrated that the JDE can be realized in the JJs constructed by the monolayer and bilayer honeycomb systems with loop current order, which directly breaks the time-reversal symmetry. For the monolayer system, the inversion symmetry can be broken by either applying a staggered sublattice potential for the HM or by reverting parts of the loop current directions to form the MHM, leading to the JDE. For the bilayer system, the JDE can be realized by applying an external electric field perpendicular to the system resulting in an electrically controllable Josephson diode, or by stacking the two layers of HMs with opposite loop current directions, which leads to an intrinsic field-free Josephson diode. Moreover, we also find that the JDE disappears when the JJ is constructed along the armchair edge which has an extra symmetry to prevent the emergence of the JDE. Finally, we demonstrate that the JDE is robust against disorder induced by impurity by calculating the average CPR for the systems with random onsite potential. The JDE persists in the average CPR over 100 random configurations and more details are shown in the supplementary material [106].

We expect this mechanism to realize the JDE can be easily applied to the other hexagonal system such as the Kagome systems. One of the possible platforms to realize this field-free JDE induced by the loop current is the Kagome metal system, which hosts a special charge density wave state as a promising candidate for the loop current order [89, 90, 93]. We hope it stimulates the exploration of the field-free JDE and expands the scope of the possible material systems to realize this effect.

This work is supported by the National Natural Science Foundation of China (NSFC) Grants No. 12274279. We gratefully acknowledge HZWTECH for providing computation facilities.

* zhangyi821@shu.edu.cn

[1] K. Jiang and J. Hu, Superconducting diode effects, *Nature Physics* **18**, 1145 (2022).

- [2] M. Nadeem, M. S. Fuhrer, and X. Wang, The superconducting diode effect, *Nature Reviews Physics* **5**, 558 (2023).
- [3] F. Ando, Y. Miyasaka, T. Li, J. Ishizuka, T. Arakawa, Y. Shiota, T. Moriyama, Y. Yanase, and T. Ono, Observation of superconducting diode effect, *Nature* **584**, 373 (2020).
- [4] L. Bauriedl, C. Bäuml, L. Fuchs, C. Baumgartner, N. Paulik, J. M. Bauer, K.-Q. Lin, J. M. Lupton, T. Taniguchi, K. Watanabe, C. Strunk, and N. Paradiso, Supercurrent diode effect and magnetochiral anisotropy in few-layer nbse₂, *Nature Communications* **13**, 4266 (2022).
- [5] J. Yun, S. Son, J. Shin, G. Park, K. Zhang, Y. J. Shin, J.-G. Park, and D. Kim, Magnetic proximity-induced superconducting diode effect and infinite magnetoresistance in a van der waals heterostructure, *Phys. Rev. Res.* **5**, L022064 (2023).
- [6] J.-X. Lin, P. Siriviboon, H. D. Scammell, S. Liu, D. Rhodes, K. Watanabe, T. Taniguchi, J. Hone, M. S. Scheurer, and J. I. A. Li, Zero-field superconducting diode effect in small-twist-angle trilayer graphene, *Nature Physics* **18**, 1221 (2022).
- [7] T. Le, Z. Pan, Z. Xu, J. Liu, J. Wang, Z. Lou, X. Yang, Z. Wang, Y. Yao, C. Wu, and X. Lin, Superconducting diode effect and interference patterns in kagome csv3sb₅, *Nature* **630**, 64 (2024).
- [8] R. Wakatsuki, Y. Saito, S. Hoshino, Y. M. Itahashi, T. Ideue, M. Ezawa, Y. Iwasa, and N. Nagaosa, Nonreciprocal charge transport in noncentrosymmetric superconductors, *Science Advances* **3**, e1602390 (2017).
- [9] Y. Miyasaka, R. Kawarazaki, H. Narita, F. Ando, Y. Ikeda, R. Hisatomi, A. Daido, Y. Shiota, T. Moriyama, Y. Yanase, and T. Ono, Observation of nonreciprocal superconducting critical field, *Applied Physics Express* **14**, 073003 (2021).
- [10] E. Zhang, X. Xu, Y.-C. Zou, L. Ai, X. Dong, C. Huang, P. Leng, S. Liu, Y. Zhang, Z. Jia, X. Peng, M. Zhao, Y. Yang, Z. Li, H. Guo, S. J. Haigh, N. Nagaosa, J. Shen, and F. Xiu, Nonreciprocal superconducting nbse₂ antenna, *Nature Communications* **11**, 5634 (2020).
- [11] Y.-Y. Lyu, J. Jiang, Y.-L. Wang, Z.-L. Xiao, S. Dong, Q.-H. Chen, M. V. Milošević, H. Wang, R. Divan, J. E. Pearson, P. Wu, F. M. Peeters, and W.-K. Kwok, Superconducting diode effect via conformal-mapped nanoholes, *Nature Communications* **12**, 2703 (2021).
- [12] H. Narita, J. Ishizuka, R. Kawarazaki, D. Kan, Y. Shiota, T. Moriyama, Y. Shimakawa, A. V. Ognev, A. S. Samardak, Y. Yanase, and T. Ono, Field-free superconducting diode effect in noncentrosymmetric superconductor/ferromagnet multilayers, *Nature Nanotechnology* **17**, 823 (2022).
- [13] E. Strambini, M. Spies, N. Ligato, S. Ilić, M. Rouco, C. González-Orellana, M. Ilyn, C. Rogero, F. S. Bergeret, J. S. Moodera, P. Virtanen, T. T. Heikkilä, and F. Giazotto, Superconducting spintronic tunnel diode, *Nature Communications* **13**, 2431 (2022).
- [14] H. Wu, Y. Wang, Y. Xu, P. K. Sivakumar, C. Pasco, U. Filippozzi, S. S. P. Parkin, Y.-J. Zeng, T. McQueen, and M. N. Ali, The field-free josephson diode in a van der waals heterostructure, *Nature* **604**, 653 (2022).
- [15] C. Baumgartner, L. Fuchs, A. Costa, S. Reinhardt, S. Gronin, G. C. Gardner, T. Lindemann, M. J. Manfra, P. E. Faria Junior, D. Kochan, J. Fabian, N. Paradiso, and C. Strunk, Supercurrent rectification and magnetochiral effects in symmetric josephson junctions, *Nature Nanotechnology* **17**, 39 (2022).
- [16] C. Baumgartner, L. Fuchs, A. Costa, J. Picó-Cortés, S. Reinhardt, S. Gronin, G. C. Gardner, T. Lindemann, M. J. Manfra, P. E. F. Junior, D. Kochan, J. Fabian, N. Paradiso, and C. Strunk, Effect of rashba and dresselhaus spin-orbit coupling on supercurrent rectification and magnetochiral anisotropy of ballistic josephson junctions, *Journal of Physics: Condensed Matter* **34**, 154005 (2022).
- [17] B. Pal, A. Chakraborty, P. K. Sivakumar, M. Davydova, A. K. Gopi, A. K. Pandeya, J. A. Krieger, Y. Zhang, M. Date, S. Ju, N. Yuan, N. B. M. Schröter, L. Fu, and S. S. P. Parkin, Josephson diode effect from cooper pair momentum in a topological semimetal, *Nature Physics* **18**, 1228 (2022).
- [18] J. Díez-Mérida, A. Díez-Carlón, S. Y. Yang, Y. M. Xie, X. J. Gao, J. Senior, K. Watanabe, T. Taniguchi, X. Lu, A. P. Higginbotham, K. T. Law, and D. K. Efetov, Symmetry-broken josephson junctions and superconducting diodes in magic-angle twisted bilayer graphene, *Nature Communications* **14**, 2396 (2023).
- [19] M. Gupta, G. V. Graziano, M. Pendharkar, J. T. Dong, C. P. Dempsey, C. Palmström, and V. S. Pribiag, Gate-tunable superconducting diode effect in a three-terminal josephson device, *Nature Communications* **14**, 3078 (2023).
- [20] B. Turini, S. Salimian, M. Carrega, A. Iorio, E. Strambini, F. Giazotto, V. Zannier, L. Sorba, and S. Heun, Josephson diode effect in high-mobility insb nanoflags, *Nano Letters* **22**, 8502 (2022).
- [21] P. Chen, G. Wang, B. Ye, J. Wang, L. Zhou, Z. Tang, L. Wang, J. Wang, W. Zhang, J. Mei, W. Chen, and H. He, Edelstein Effect Induced Superconducting Diode Effect in Inversion Symmetry Breaking MoTe₂ Josephson Junctions, *Advanced Functional Materials* **34**, 2311229 (2024).
- [22] S. Ghosh, V. Patil, A. Basu, Kuldeep, A. Dutta, D. A. Jangade, R. Kulkarni, A. Thamizhavel, J. F. Steiner, F. von Oppen, and M. M. Deshmukh, High-temperature Josephson diode, *Nature Materials* **23**, 612 (2024).
- [23] N. Lotfizadeh, W. F. Schiela, B. Pekerten, P. Yu, B. H. Elfeky, W. M. Strickland, A. Matos-Abiague, and J. Shabani, Superconducting diode effect sign change in epitaxial Al-InAs Josephson junctions, *Communications Physics* **7**, 1 (2024).
- [24] J.-K. Kim, K.-R. Jeon, P. K. Sivakumar, J. Jeon, C. Koerner, G. Woltersdorf, and S. S. P. Parkin, Intrinsic supercurrent nonreciprocity coupled to the crystal structure of a van der Waals Josephson barrier, *Nature Communications* **15**, 1120 (2024).
- [25] J. Hu, C. Wu, and X. Dai, Proposed design of a josephson diode, *Phys. Rev. Lett.* **99**, 067004 (2007).
- [26] A. Buzdin, Direct coupling between magnetism and superconducting current in the josephson ϕ_0 junction, *Phys. Rev. Lett.* **101**, 107005 (2008).
- [27] Z. Huang and X. Hu, Josephson effects in three-band superconductors with broken time-reversal symmetry, *Applied Physics Letters* **104**, 162602 (2014).
- [28] T. Yokoyama, M. Eto, and Y. V. Nazarov, Anomalous josephson effect induced by spin-orbit interaction and zeeman effect in semiconductor nanowires, *Phys. Rev. B* **89**, 195407 (2014).
- [29] F. Dolcini, M. Houzet, and J. S. Meyer, Topological josephson ϕ_0 junctions, *Phys. Rev. B* **92**, 035428 (2015).
- [30] D. B. Szombati, S. Nadj-Perge, D. Car, S. R. Plissard, E. P. A. M. Bakkers, and L. P. Kouwenhoven, Josephson ϕ_0 -junction in nanowire quantum dots, *Nature Physics* **12**, 568 (2016).
- [31] A. Assouline, C. Feuillet-Palma, N. Bergeal, T. Zhang, A. Mottaghizadeh, A. Zimmers, E. Lhuillier, M. Eddrie, P. Atkinson, M. Aprili, and H. Aubin, Spin-orbit induced phase-shift in bi₂se₃ josephson junctions, *Nature Communications* **10**, 126 (2019).
- [32] M. Alidoust and J. Linder, φ -state and inverted fraunhofer pattern in nonaligned josephson junctions, *Phys. Rev. B* **87**, 060503 (2013).
- [33] I. V. Bobkova, A. M. Bobkov, A. A. Zyuzin, and M. Alidoust,

- Magnetolectrics in disordered topological insulator Josephson junctions, *Phys. Rev. B* **94**, 134506 (2016).
- [34] M. Alidoust and H. Hamzeshpour, Spontaneous supercurrent and φ_0 phase shift parallel to magnetized topological insulator interfaces, *Phys. Rev. B* **96**, 165422 (2017).
- [35] M. Alidoust, M. Willatzen, and A.-P. Jauho, Strain-engineered Majorana zero energy modes and φ_0 Josephson state in black phosphorus, *Phys. Rev. B* **98**, 085414 (2018).
- [36] M. Alidoust, Critical supercurrent and φ_0 state for probing a persistent spin helix, *Phys. Rev. B* **101**, 155123 (2020).
- [37] M. Alidoust, C. Shen, and I. Žutić, Cubic spin-orbit coupling and anomalous Josephson effect in planar junctions, *Phys. Rev. B* **103**, L060503 (2021).
- [38] K. Halterman, M. Alidoust, R. Smith, and S. Starr, Supercurrent diode effect, spin torques, and robust zero-energy peak in planar half-metallic trilayers, *Phys. Rev. B* **105**, 104508 (2022).
- [39] K. Misaki and N. Nagaosa, Theory of the nonreciprocal Josephson effect, *Phys. Rev. B* **103**, 245302 (2021).
- [40] J. J. He, Y. Tanaka, and N. Nagaosa, A phenomenological theory of superconductor diodes, *New Journal of Physics* **24**, 053014 (2022).
- [41] N. F. Q. Yuan and L. Fu, Supercurrent diode effect and finite-momentum superconductors, *Proceedings of the National Academy of Sciences* **119**, e2119548119 (2022).
- [42] A. Daido, Y. Ikeda, and Y. Yanase, Intrinsic superconducting diode effect, *Phys. Rev. Lett.* **128**, 037001 (2022).
- [43] M. Davydova, S. Prembabu, and L. Fu, Universal Josephson diode effect, *Science Advances* **8**, eabo0309 (2022).
- [44] H. D. Scammell, J. I. A. Li, and M. S. Scheurer, Theory of zero-field superconducting diode effect in twisted trilayer graphene, *2D Materials* **9**, 025027 (2022).
- [45] Y. Zhang, Y. Gu, P. Li, J. Hu, and K. Jiang, General Theory of Josephson Diodes, *Physical Review X* **12**, 041013 (2022).
- [46] R. S. Souto, M. Leijnse, and C. Schrade, Josephson diode effect in supercurrent interferometers, *Phys. Rev. Lett.* **129**, 267702 (2022).
- [47] T. Karabassov, I. V. Bobkova, A. A. Golubov, and A. S. Vasenko, Hybrid helical state and superconducting diode effect in superconductor/ferromagnet/topological insulator heterostructures, *Phys. Rev. B* **106**, 224509 (2022).
- [48] J.-X. Hu, Z.-T. Sun, Y.-M. Xie, and K. T. Law, Josephson diode effect induced by valley polarization in twisted bilayer graphene, *Phys. Rev. Lett.* **130**, 266003 (2023).
- [49] B. Lu, S. Ikegaya, P. Bursset, Y. Tanaka, and N. Nagaosa, Tunable Josephson diode effect on the surface of topological insulators, *Phys. Rev. Lett.* **131**, 096001 (2023).
- [50] M. Alvarado, P. Bursset, and A. L. Yeyati, Intrinsic nonmagnetic ϕ_0 Josephson junctions in twisted bilayer graphene, *Phys. Rev. Res.* **5**, L032033 (2023).
- [51] K. Nakamura, A. Daido, and Y. Yanase, Orbital effect on the intrinsic superconducting diode effect, *Phys. Rev. B* **109**, 094501 (2024).
- [52] J. Wang, Y. Jiang, J. J. Wang, and J.-F. Liu, Efficient Josephson diode effect on a two-dimensional topological insulator with asymmetric magnetization, *Physical Review B* **109**, 075412 (2024).
- [53] J. Cayao, N. Nagaosa, and Y. Tanaka, Enhancing the Josephson diode effect with Majorana bound states, *Physical Review B* **109**, L081405 (2024).
- [54] A. Soori, Josephson diode effect in junctions of superconductors with band asymmetric metals, *Journal of Physics: Condensed Matter* **36**, 335303 (2024).
- [55] P. A. Volkov, É. Lantagne-Hurtubise, T. Tummuru, S. Plugge, J. H. Pixley, and M. Franz, Josephson diode effects in twisted nodal superconductors, *Physical Review B* **109**, 094518 (2024).
- [56] J. J. Cuzzo, W. Pan, J. Shabani, and E. Rossi, Microwave-tunable diode effect in asymmetric SQUIDs with topological Josephson junctions, *Physical Review Research* **6**, 023011 (2024).
- [57] R. Seoane Souto, M. Leijnse, C. Schrade, M. Valentini, G. Katsaros, and J. Danon, Tuning the Josephson diode response with an ac current, *Physical Review Research* **6**, L022002 (2024).
- [58] D. Debnath and P. Dutta, Gate-tunable Josephson diode effect in Rashba spin-orbit coupled quantum dot junctions, *Physical Review B* **109**, 174511 (2024).
- [59] J. S. Meyer and M. Houzet, Josephson diode effect in a ballistic single-channel nanowire (2024), arXiv:2404.01429 [cond-mat].
- [60] S. Fracassi, S. Traverso, N. T. Ziani, M. Carrega, S. Heun, and M. Sassetti, Anomalous supercurrent and diode effect in locally perturbed topological Josephson junctions (2024), arXiv:2403.17894 [cond-mat].
- [61] A. Zazunov, J. Rech, T. Jonckheere, B. Grémaud, T. Martin, and R. Egger, Nonreciprocal charge transport and subharmonic structure in voltage-biased Josephson diodes, *Physical Review B* **109**, 024504 (2024).
- [62] H. Huang, T. de Picoli, and J. I. Väyrynen, Superconducting Diode Effect in Two-dimensional Topological Insulator Edges and Josephson Junctions (2024), arXiv:2404.14566 [cond-mat].
- [63] T. Karabassov, Anisotropic Josephson Diode Effect in the Topological Hybrid Junctions with the Hexagonal Warping, *JETP Letters* **119**, 316 (2024).
- [64] J. H. Correa and M. P. Nowak, Theory of universal diode effect in three-terminal Josephson junctions (2024), arXiv:2401.16262 [cond-mat].
- [65] A. Greco, Q. Pichard, E. Strambini, and F. Giazotto, Double loop dc-SQUID as a tunable Josephson diode (2024), arXiv:2404.05521 [cond-mat].
- [66] D. Margineda, A. Crippa, E. Strambini, Y. Fukaya, M. T. Mercaldo, M. Cuoco, and F. Giazotto, Sign reversal diode effect in superconducting dayem nanobridges, *Communications Physics* **6**, 343 (2023).
- [67] D. Margineda, A. Crippa, E. Strambini, L. Borgongino, A. Paggi, G. de Simoni, L. Sorba and Yuri Fukaya, M. T. Mercaldo, C. Ortix, M. Cuoco, and F. Giazotto, Back-action supercurrent diodes, arXiv e-prints, arXiv:2311.14503 (2023), arXiv:2311.14503.
- [68] Y. Fukaya, M. T. Mercaldo, D. Margineda, A. Crippa, E. Strambini, F. Giazotto, C. Ortix, and M. Cuoco, Design of supercurrent diode by vortex phase texture, arXiv e-prints, arXiv:2403.04421 (2024), arXiv:2403.04421.
- [69] P.-H. Fu, Y. Xu, S. A. Yang, C. H. Lee, Y. S. Ang, and J.-F. Liu, Field-effect Josephson diode via asymmetric spin-momentum locking states, *Phys. Rev. Appl.* **21**, 054057 (2024).
- [70] P.-H. Fu, Y. Xu, J.-F. Liu, C. H. Lee, and Y. Sin Ang, Transverse Cooper-Pair Rectifier, arXiv e-prints, arXiv:2405.04751 (2024), arXiv:2405.04751.
- [71] Y. Zhang and Z. Wang, Kramers full-ferrell state and superconducting spin diode effect, *Phys. Rev. B* **107**, 224510 (2023).
- [72] Y. Mao, Q. Yan, Y.-C. Zhuang, and Q.-F. Sun, Universal spin superconducting diode effect from spin-orbit coupling, *Phys. Rev. Lett.* **132**, 216001 (2024).
- [73] F. D. M. Haldane, Model for a quantum hall effect without

- landau levels: Condensed-matter realization of the "parity anomaly", *Phys. Rev. Lett.* **61**, 2015 (1988).
- [74] I. Affleck and J. B. Marston, Large- n limit of the heisenberg-hubbard model: Implications for high- T_c superconductors, *Phys. Rev. B* **37**, 3774 (1988).
- [75] M. U. Ubbens and P. A. Lee, Flux phases in the t-j model, *Phys. Rev. B* **46**, 8434 (1992).
- [76] P. A. Lee, N. Nagaosa, and X.-G. Wen, Doping a mott insulator: Physics of high-temperature superconductivity, *Rev. Mod. Phys.* **78**, 17 (2006).
- [77] C. M. Varma, Non-fermi-liquid states and pairing instability of a general model of copper oxide metals, *Phys. Rev. B* **55**, 14554 (1997).
- [78] C. M. Varma, Pseudogap phase and the quantum-critical point in copper-oxide metals, *Phys. Rev. Lett.* **83**, 3538 (1999).
- [79] S. Chakravarty, R. B. Laughlin, D. K. Morr, and C. Nayak, Hidden order in the cuprates, *Phys. Rev. B* **63**, 094503 (2001).
- [80] C. Nayak, Density-wave states of nonzero angular momentum, *Phys. Rev. B* **62**, 4880 (2000).
- [81] J. W. F. Venderbos, Symmetry analysis of translational symmetry broken density waves: Application to hexagonal lattices in two dimensions, *Phys. Rev. B* **93**, 115107 (2016).
- [82] J. Liu, S. Y. Park, K. F. Garrity, and D. Vanderbilt, Flux states and topological phases from spontaneous time-reversal symmetry breaking in CrSi(Ge)Te₃-based systems, *Phys. Rev. Lett.* **117**, 257201 (2016).
- [83] L. Classen, C. Honerkamp, and M. M. Scherer, Competing phases of interacting electrons on triangular lattices in moiré heterostructures, *Phys. Rev. B* **99**, 195120 (2019).
- [84] Y. Chen, K. Jiang, Y. Zhang, and J. Hu, Flux phases in the extended hubbard model on the triangular lattice, *Science China Physics, Mechanics & Astronomy* **67**, 297211 (2024).
- [85] B. R. Ortiz, S. M. L. Teicher, Y. Hu, J. L. Zuo, P. M. Sarte, E. C. Schueller, A. M. M. Abeykoon, M. J. Krogstad, S. Rosenkranz, R. Osborn, R. Seshadri, L. Balents, J. He, and S. D. Wilson, CsV₃Sb₅: A \mathbb{Z}_2 topological kagome metal with a superconducting ground state, *Phys. Rev. Lett.* **125**, 247002 (2020).
- [86] B. R. Ortiz, S. M. L. Teicher, L. Kautzsch, P. M. Sarte, N. Ratcliff, J. Harter, J. P. C. Ruff, R. Seshadri, and S. D. Wilson, Fermi surface mapping and the nature of charge-density-wave order in the kagome superconductor CsV₃Sb₅, *Phys. Rev. X* **11**, 041030 (2021).
- [87] Z. Liang, X. Hou, F. Zhang, W. Ma, P. Wu, Z. Zhang, F. Yu, J.-J. Ying, K. Jiang, L. Shan, Z. Wang, and X.-H. Chen, Three-dimensional charge density wave and surface-dependent vortex-core states in a kagome superconductor CsV₃Sb₅, *Phys. Rev. X* **11**, 031026 (2021).
- [88] E. Uykur, B. R. Ortiz, O. Iakutkina, M. Wenzel, S. D. Wilson, M. Dressel, and A. A. Tsirlin, Low-energy optical properties of the nonmagnetic kagome metal CsV₃Sb₅, *Phys. Rev. B* **104**, 045130 (2021).
- [89] N. Shumiya, M. S. Hossain, J.-X. Yin, Y.-X. Jiang, B. R. Ortiz, H. Liu, Y. Shi, Q. Yin, H. Lei, S. S. Zhang, G. Chang, Q. Zhang, T. A. Cochran, D. Multer, M. Litskevich, Z.-J. Cheng, X. P. Yang, Z. Guguchia, S. D. Wilson, and M. Z. Hasan, Intrinsic nature of chiral charge order in the kagome superconductor RbV₃Sb₅, *Phys. Rev. B* **104**, 035131 (2021).
- [90] Y.-X. Jiang, J.-X. Yin, M. M. Denner, N. Shumiya, B. R. Ortiz, G. Xu, Z. Guguchia, J. He, M. S. Hossain, X. Liu, J. Ruff, L. Kautzsch, S. S. Zhang, G. Chang, I. Belopolski, Q. Zhang, T. A. Cochran, D. Multer, M. Litskevich, Z.-J. Cheng, X. P. Yang, Z. Wang, R. Thomale, T. Neupert, S. D. Wilson, and M. Z. Hasan, Unconventional chiral charge order in kagome superconductor KV₃Sb₅, *Nature Materials* **20**, 1353 (2021).
- [91] H. Zhao, H. Li, B. R. Ortiz, S. M. L. Teicher, T. Park, M. Ye, Z. Wang, L. Balents, S. D. Wilson, and I. Zeljkovic, Cascade of correlated electron states in the kagome superconductor CsV₃Sb₅, *Nature* **599**, 216 (2021).
- [92] H. Li, H. Zhao, B. R. Ortiz, T. Park, M. Ye, L. Balents, Z. Wang, S. D. Wilson, and I. Zeljkovic, Rotation symmetry breaking in the normal state of a kagome superconductor KV₃Sb₅, *Nature Physics* **18**, 265 (2022).
- [93] Y. Xing, S. Bae, E. Ritz, F. Yang, T. Birol, A. N. Capa Salinas, B. R. Ortiz, S. D. Wilson, Z. Wang, R. M. Fernandes, and V. Madhavan, Optical manipulation of the charge-density-wave state in rbv₃sb₅, *Nature* **631**, 60 (2024).
- [94] X. Feng, K. Jiang, Z. Wang, and J. Hu, Chiral flux phase in the kagome superconductor AV₃Sb₅, *Science Bulletin* **66**, 1384 (2021).
- [95] M. M. Denner, R. Thomale, and T. Neupert, Analysis of charge order in the kagome metal AV₃Sb₅ ($A = K, Rb, Cs$), *Phys. Rev. Lett.* **127**, 217601 (2021).
- [96] T. Park, M. Ye, and L. Balents, Electronic instabilities of kagome metals: Saddle points and Landau theory, *Phys. Rev. B* **104**, 035142 (2021).
- [97] Y.-P. Lin and R. M. Nandkishore, Complex charge density waves at van hove singularity on hexagonal lattices: Haldane-model phase diagram and potential realization in the kagome metals AV₃Sb₅ ($A = K, Rb, Cs$), *Phys. Rev. B* **104**, 045122 (2021).
- [98] Y. Gu, Y. Zhang, X. Feng, K. Jiang, and J. Hu, Gapless excitations inside the fully gapped kagome superconductors AV₃Sb₅, *Phys. Rev. B* **105**, L100502 (2022).
- [99] J.-W. Dong, Z. Wang, and S. Zhou, Loop-current charge density wave driven by long-range coulomb repulsion on the kagomé lattice, *Phys. Rev. B* **107**, 045127 (2023).
- [100] S. Zhou and Z. Wang, Chern fermi pocket, topological pair density wave, and charge-4e and charge-6e superconductivity in kagomé superconductors, *Nature Communications* **13**, 7288 (2022).
- [101] R. Tazai, Y. Yamakawa, and H. Kontani, Charge-loop current order and \mathbb{Z}_3 nematicity mediated by bond order fluctuations in kagome metals, *Nature Communications* **14**, 7845 (2023).
- [102] R.-Q. Fu, J. Zhan, M. Dürrnagel, H. Hohmann, R. Thomale, J. Hu, Z. Wang, S. Zhou, and X. Wu, Exotic charge density waves and superconductivity on the Kagome Lattice, *arXiv e-prints*, arXiv:2405.09451 (2024).
- [103] E. Colomé and M. Franz, Antichiral Edge States in a Modified Haldane Nanoribbon, *Phys. Rev. Lett.* **120**, 086603 (2018).
- [104] L. Zhu, V. Aji, and C. M. Varma, Ordered loop current states in bilayer graphene, *Physical Review B* **87**, 035427 (2013).
- [105] C. W. J. Beenakker, Universal limit of critical-current fluctuations in mesoscopic Josephson junctions, *Phys. Rev. Lett.* **67**, 3836 (1991).
- [106] See Supplemental Material for more detailed discussions.

Supplemental Material: Josephson diodes induced by the loop current states

CONSTRUCTION OF THE HAMILTONIAN OF A JOSEPHSON JUNCTION

We study a planar Josephson junction (JJ) in which the width of the junction spans N_y unit cells. The two superconducting regions each have a length of N_s unit cells, while the central non-superconducting region extends over N_n unit cells as shown in Fig. S1. Thus the Hamiltonian of the JJ can be expressed as

$$\begin{aligned}
H &= H_{SL} + H_{SN} + H_N + H_{NS} + H_{SR} \\
H_{SL} &= H_0 + \Delta e^{i\varphi} \sum_i c_{i\uparrow}^\dagger c_{i\downarrow}^\dagger + h.c. - \mu_0 \sum_{i,\sigma} c_{i\sigma}^\dagger c_{i\sigma} \\
H_N &= H_0 - \mu_0 \sum_{i,\sigma} c_{i\sigma}^\dagger c_{i\sigma} \\
H_{SR} &= H_0 + \Delta \sum_i c_{i\uparrow}^\dagger c_{i\downarrow}^\dagger + h.c. - \mu_0 \sum_{i,\sigma} c_{i\sigma}^\dagger c_{i\sigma} \\
H_{SN} &= -t \sum_{\langle(i,j)\rangle\sigma, i \in SL, j \in N} c_{i\sigma}^\dagger c_{j\sigma} + t_1 \sum_{\langle\langle(i,j)\rangle\rangle\sigma, i \in SL, j \in N} e^{-iv_{ij}\phi} c_{i\sigma}^\dagger c_{j\sigma} + h.c. \\
H_{NS} &= -t \sum_{\langle(i,j)\rangle\sigma, i \in N, j \in SR} c_{i\sigma}^\dagger c_{j\sigma} + t_1 \sum_{\langle\langle(i,j)\rangle\rangle\sigma, i \in N, j \in SR} e^{-iv_{ij}\phi} c_{i\sigma}^\dagger c_{j\sigma} + h.c.
\end{aligned} \tag{S1}$$

where H_0 represents the Hamiltonian of monolayer (H_m) or bilayer (H_b) system. For the monolayer system, it can be written as

$$H_m = -t \sum_{\langle(i,j)\rangle\sigma} c_{i\sigma}^\dagger c_{j\sigma} - t_1 \sum_{\langle\langle(i,j)\rangle\rangle\sigma} e^{-iv_{ij}\phi} c_{i\sigma}^\dagger c_{j\sigma} \tag{S2}$$

describing the monolayer Haldane or modified Haldane models. For the bilayer system, it can be expressed as

$$\begin{aligned}
H_b &= H_1 + H_2 + H_{12} \\
H_1 &= -t \sum_{\langle(i,j)\rangle\sigma} c_{i\sigma}^\dagger c_{j\sigma} - t_1 \sum_{\langle\langle(i,j)\rangle\rangle\sigma} e^{-iv_{ij}\phi} c_{i\sigma}^\dagger c_{j\sigma} \\
H_{12} &= -t_\perp \sum_{i,\sigma} c_{i,A1\sigma}^\dagger c_{i,B2\sigma} + h.c.
\end{aligned} \tag{S3}$$

describing the bilayer Haldane or modified Haldane model coupled through the interlayer coupling t_\perp . Thus, H_{SL} and H_{SR} correspond to the Hamiltonian of the superconducting region on the left and right sides. H_N describes the normal region in the middle with the superconducting pairing term set to 0. H_{SN} and H_{NS} correspond to the spin-conserving hoppings between the superconducting and normal sections which include both the nearest-neighbor and next-nearest-neighbor hoppings and take the same values and patterns as those in the normal region. The superconducting phase bias for the JJ is assigned to the left superconducting region as φ so that the phase in the right superconducting region is set to 0. The amplitude of the order parameter is taken as $\Delta = 0.2t$ for all calculations in this paper. μ_0 represents the chemical potential of the entire material, which is set to $-0.4t$ in the bilayer model, and set to 0 in the monolayer system. Moreover, a staggered lattice potential can be described by an extra term $H_s = V_s \sum_{i,\sigma} (c_{i,A\sigma}^\dagger c_{i,A\sigma} - c_{i,B\sigma}^\dagger c_{i,B\sigma})$ added into the monolayer Hamiltonian and an out-of-plane electric field for the bilayer system can be described by a term $H_U = U/2 \sum_{i,\sigma} (-1)^i c_{i\sigma}^\dagger c_{i\sigma}$. The periodic boundary condition is adopted along the width of the junction and the total Hamiltonian is diagonalized numerically. Then the Josephson currents can be calculated as

$$I(\varphi) = \frac{2e}{\hbar} \partial_\varphi \sum_n f(\epsilon_n(\varphi)) \epsilon_n(\varphi) \tag{S4}$$

with $\epsilon_n(\varphi)$ the n th eigenvalue for $H(\varphi)$ and $f(\epsilon)$ the Fermi distribution function.

CPR FOR THE JJ CONSTRUCTED BY THE MONOLAYER HM MODEL

For the JJ constructed by the monolayer HM model, the CPR shows no diode effect since the HM model has the inversion symmetry (C_2 for the monolayer system) as shown in Fig. S2.

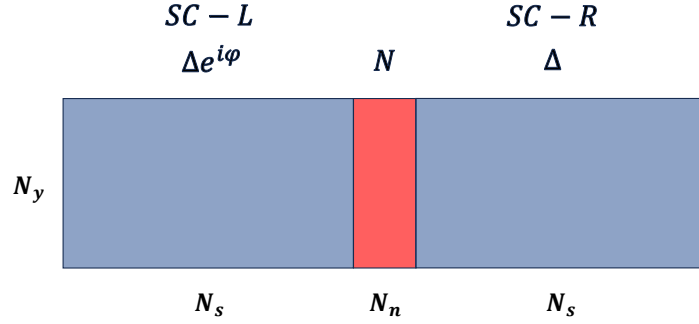


FIG. S1. Schematic of a JJ. The lengths of the left and the right superconductors are both N_s and the middle non-superconducting region is N_n . The width of the junction is N_y unit cells. The superconducting phase bias φ for the JJ is assigned to the left superconducting region, with the phase of the right superconducting region set to 0.

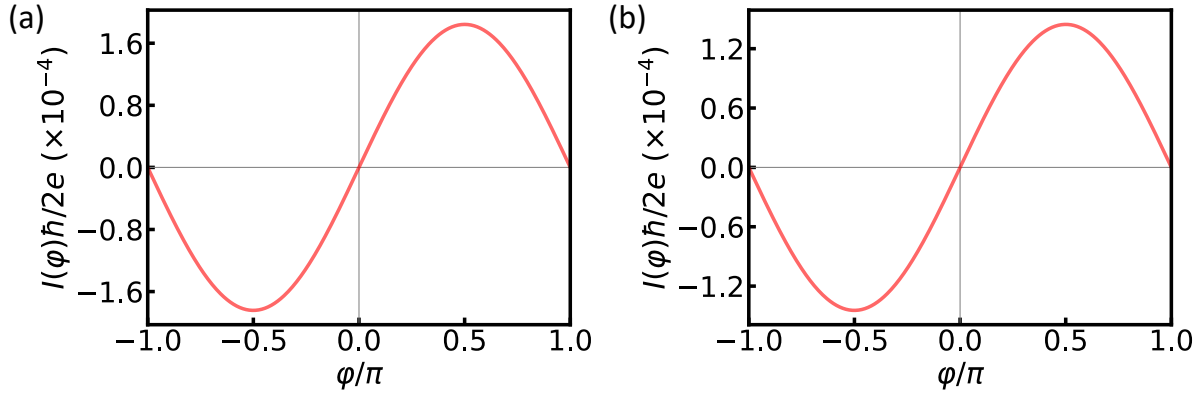


FIG. S2. The CPR of the JJ constructed by the monolayer HM. (a) The JJ is along the zigzag edge direction and (b) the JJ is along the armchair edge direction. Parameters are taken as $t = 1$, $t_1 = 0.4t$, $\phi = \pi/4$, $\Delta = 0.2t$, $\mu_0 = 0$

CPR FOR THE ARMCHAIR JJ CONSTRUCTED BY THE BILAYER MODELS

As mentioned in the main text, the JDE can be achieved by applying an out-of-plane electric field to the bilayer HMs with the same loop current direction or stacking the two layers of the HMs with opposite loop current directions in the zigzag JJs. However, if the JJs are constructed along the armchair edge, the JDE for both cases disappears, which is related to the mirror symmetry of the armchair JJs. Here, we provide the numerical evidence to verify these results in Fig. S3, where the Josephson current of the armchair JJ $I(\varphi)$ is an odd function of the phase bias φ and thus does not show any diode effect.

THE INFLUENCE OF THE CHEMICAL POTENTIAL μ_0 AND PAIRING STRENGTH Δ ON THE DIODE EFFICIENCY η

To explore the effect the chemical potential μ_0 and the pairing amplitude Δ to the diode efficiency η , we calculate η for various values of $\frac{\Delta}{t}$ and $\frac{\mu_0}{t}$. The pairing amplitude Δ is varied from 0 to $0.4t$ and the chemical potential μ_0 is varied from $-0.5t$ to $0.5t$ in the bilayer model with other parameters unchanged. The results are shown in Fig. S4 where the parameters selected in the paper are marked with black dots. We can see that the diode efficiency η increases significantly when $\mu_0 < -0.3t$ and weak Δ , while it remains relatively low in other parameter regions.

THE IMPACT OF IMPURITY SCATTERING

To investigate the impact of impurities on the diode effect, we introduced a random potential into the model to simulate the influence of impurities. We added random potentials obeying the uniform distribution ranging from $-\frac{W}{2}$ to $\frac{W}{2}$ to each atom

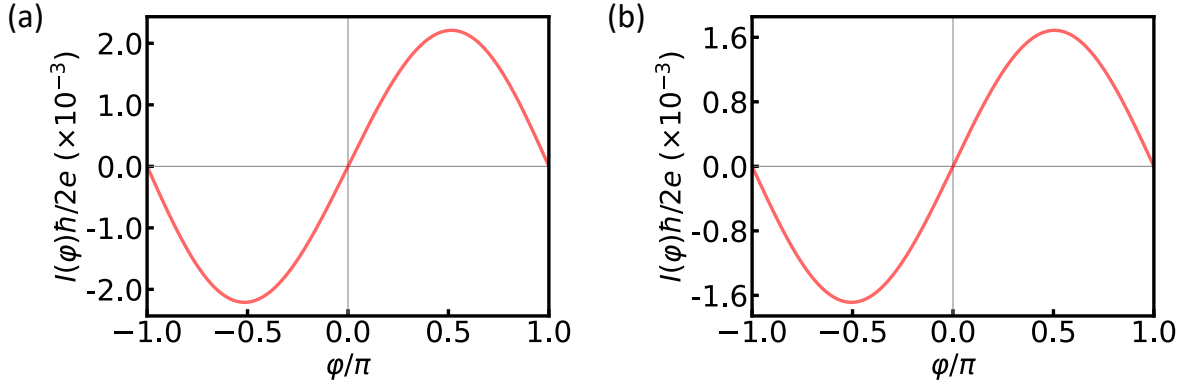


FIG. S3. The CPR in bilayer armchair HMs. (a) The JJ is formed by stacking two HMs with the same loop current direction and an external electric field perpendicular to the system is applied. (b) The JJ is formed by stacking two HMs with opposite loop current directions. Parameters are taken as $t = 1$, $t_1 = 0.4t$, $t_{\perp} = 0.4t$, $\phi = \pi/4$, $\Delta = 0.2t$, $\mu_0 = -0.2t$

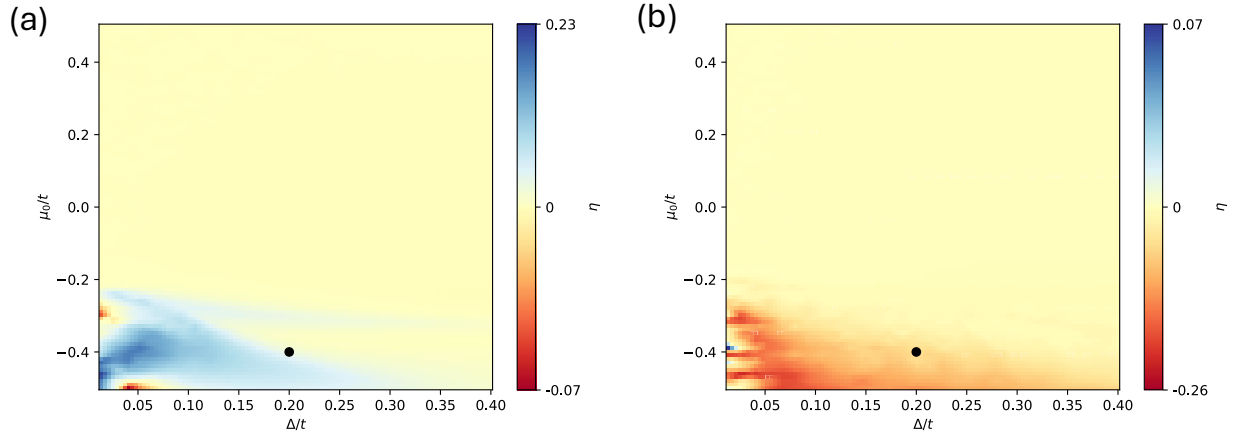


FIG. S4. The calculated diode efficiency η for different values of μ_0 and Δ . The red region indicates η is negative, the blue region indicates η is positive, and the yellow region represents regions where the JDE is not significant but still present. The black dots mark the parameters selected in the main text, as in Fig.4(a)(b). (a) The JJ is formed by stacking two HMs with the same loop current direction. Inversion symmetry is broken by applying voltage ($U = 0.5t$) between the two layers. (b) The JJ is formed by stacking two HMs with opposite loop current directions. Parameters are taken as $t = 1$, $t_1 = 0.4t$, $t_{\perp} = 0.4t$, $\phi = \pi/4$, $\Delta = 0.2t$, $\mu_0 = -0.4t$.

in the monolayer MHM and performed 100 calculations to obtain the average. Since the translation invariance along the y -direction is broken by the random impurity potential, we perform the calculation in real space, which significantly increases the computational complexity. To address this, we reduce the model size. The size in the x -direction remains unchanged, while in the y -direction, it is reduced from 100 “unit cells”(4*100 atoms) to 10 “unit cells”(4*10 atoms). In Fig. S5, we compare the averaged CPR and diode efficiency η obtained from the disordered models with different disorder strength W to those of the impurity-free model. The results clearly show that the diode effect persists with the increase of the disorder strength, indicating that the diode effect is robust against the disorder.

SYMMETRY ANALYSIS

In this section, we demonstrate the reason why the JDE realized in the zigzag JJs disappears in the armchair JJs. From the symmetry perspective, if the system remains invariant under a certain operation that simultaneously changes the sign of the current operator, it implies that the critical current must have the same magnitude in opposite directions, resulting in the absence of the JDE. We find that such symmetry operations can be constructed by the following three operations: the mirror reflection

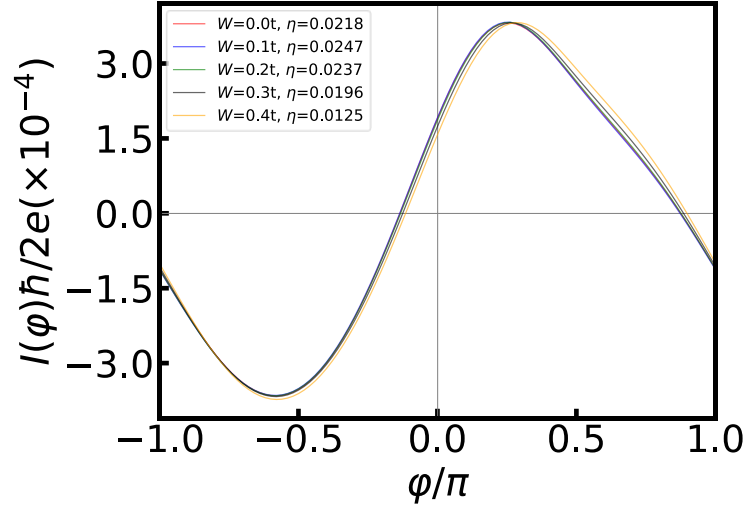


FIG. S5. The CPR and the diode efficiency η various disorder strength W . The three CPR curves for $W = 0t, 0.1t, 0.2t$ overlap due to the minimal offsets.

(M_i), the time-reversal (\mathcal{T}) and inversion (C_2 in monolayer model). Both the C_2 and \mathcal{T} operations can change the current direction. M_i represents the mirror reflection about the plane perpendicular to the i -axis, and the definition of the directions is schematically shown in Fig. S6, where $i = a$ corresponds to the zigzag direction and $i = b$ represents the armchair direction. For the zigzag JJ, M_a changes the current direction while M_b does not. Conversely, for the armchair JJ, M_b changes the current direction, but M_a does not.

For JJs constructed by different models with different junction directions, the possible symmetry operations that prevent the emergence of the JDE are summarized in Table. I. For example, for the armchair JJ constructed by the HM model with staggered lattice potential, operations M_b , C_2 and \mathcal{T} all change the direction of the current. Therefore, the combined operation $M_b * C_2 * \mathcal{T}$ changes the direction of the current while keeping the system invariant. Hence, the JDE is absent in the armchair JJ constructed by the HM model with staggered lattice potential. For zigzag JJ constructed by the same model, we can not find any symmetry operations that also change the direction of the current which is represented by the ‘ \times ’ sign in the table.

monolayer	operations	JDE
armchair HM	C_2	No
armchair MHM	M_b	No
zigzag HM	C_2	No
zigzag MHM	\times	Yes
monolayer with staggered potential	operations	JDE
armchair HM	$M_b * C_2 * \mathcal{T}$	No
armchair MHM	$M_b * C_2 * \mathcal{T}$	No
zigzag HM	\times	Yes
zigzag MHM	\times	Yes
bilayer HMs with same current direction and interlayer potential	operations	JDE
armchair HMs	$M_b * C_2 * \mathcal{T}$	No
zigzag HMs	\times	Yes
bilayer HMs with opposite current direction	operations	JDE
armchair HMs	$M_b * C_2 * \mathcal{T}$	No
zigzag HMs	\times	Yes

TABLE I. Symmetry analysis for the JDE. The first column lists all the models used to construct the Josephson junction, the second column lists the symmetry operations that prevent the emergence of the JDE where the ‘ \times ’ sign means no such symmetry operation and the last column shows whether certain Josephson junction can show the JDE or not.

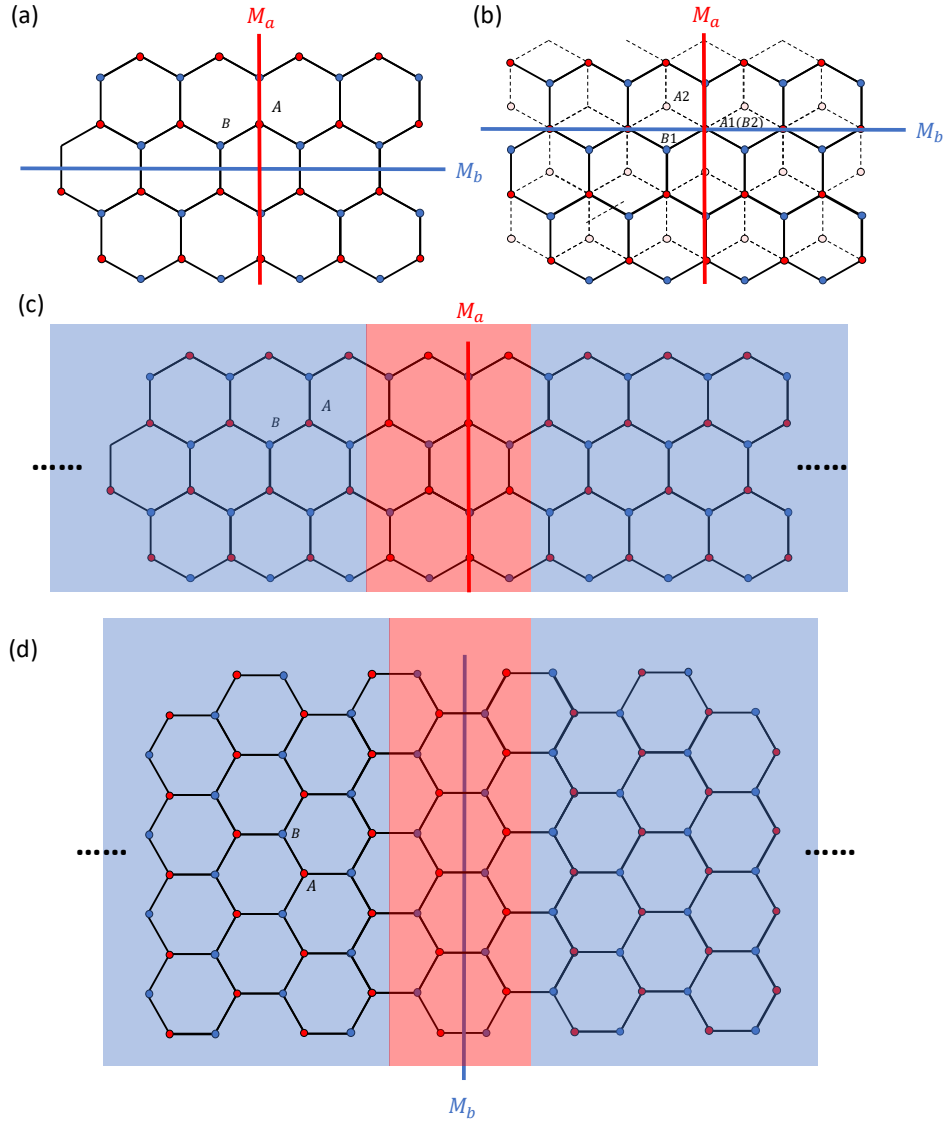


FIG. S6. Mirror reflection operation in the monolayer model (a) and the bilayer model (b). (c) M_a changes the current direction along the zigzag edge direction in the monolayer model. (d) M_b changes the current along the armchair edge direction in the monolayer model. The construction of the bilayer model is similar to that of the monolayer model.